A dynamic bead-based microarray for parallel DNA detection

2011 J. Micromech. Microeng. 21 054019

(http://iopscience.iop.org/0960-1317/21/5/054019)

J. Micromech. Microeng. **21** (2011) 054019 (8pp) doi:10.1088/0960-1317/21/5/054019

A dynamic bead-based microarray for parallel DNA detection

R D Sochol[1], B P Casavant[2], M E Dueck[2], L P Lee[2] and L Lin[1]

[1] Department of Mechanical Engineering, Berkeley Sensor and Actuator Center, Biomolecular Nanotechnology Center, University of California, Berkeley, CA 94720, USA
[2] Department of Bioengineering, Berkeley Sensor and Actuator Center, Biomolecular Nanotechnology Center, University of California, Berkeley, CA 94720, USA

E-mail: rsochol@gmail.com

Received 1 November 2010, in final form 24 January 2011
Published 28 April 2011
Online at stacks.iop.org/JMM/21/054019

Abstract
A microfluidic system has been designed and constructed by means of micromachining processes to integrate both microfluidic mixing of mobile microbeads and hydrodynamic microbead arraying capabilities on a single chip to simultaneously detect multiple bio-molecules. The prototype system has four parallel reaction chambers, which include microchannels of 18 × 50 μm^2 cross-sectional area and a microfluidic mixing section of 22 cm length. Parallel detection of multiple DNA oligonucleotide sequences was achieved via molecular beacon probes immobilized on polystyrene microbeads of 16 μm diameter. Experimental results show quantitative detection of three distinct DNA oligonucleotide sequences from the Hepatitis C viral (HCV) genome with single base-pair mismatch specificity. Our dynamic bead-based microarray offers an effective microfluidic platform to increase parallelization of reactions and improve microbead handling for various biological applications, including bio-molecule detection, medical diagnostics and drug screening.

1. Introduction

The advancement of microfluidic platforms for surface-based biochemical assays impacts a broad range of biomedical fields, including genomics, proteomics, drug discovery, and infectious disease diagnostics [1, 2]. System miniaturization results in a variety of benefits, including high surface-to-volume ratios, low reagent volumes, and rapid diffusion times. As a result, there have been significant developments in two primary classes of microfluidic arrays: (i) static microarrays, which consist of bio-molecules immobilized on static substrates, and (ii) dynamic microarrays, which consist of bio-molecules immobilized on mobile substrates, such as microbeads [2–5]. Bead-based microfluidic platforms have attracted significant attention in recent years due to their enhanced reaction kinetics, reduced background noise, and decreased system costs [2–8]. Furthermore, multiplexed reactions could be implemented in these microfluidic platforms to increase throughput for bead-based microarrays [7–9].

Previously, bead-based assays have been developed to achieve microfluidic mixing and visualization with either mobile or non-mobile microbeads. For mobile (i.e. dynamic) bead-based microarrays, microbeads suspended in a solution undergo microfluidic mixing with reagents and are then visualized dynamically (e.g., via flow cytometry) for detection [7, 10]. In such systems, the microbeads are never immobilized during the fluidic reaction process. In contrast, non-mobile (i.e. fixed) bead-based arrays consist of microbeads that are first immobilized in microfluidic systems (e.g., using microwells or wier structures), and then fluidic reagents are delivered to the non-mobile beads [11–17]. In this work, we incorporate these two techniques into a single system capable of achieving: (i) dynamic mixing of mobile microbeads with distinct reagents, and then (ii) microbead immobilization for visualization and signal detection.

By integrating controlled microfluidic mixing of suspended microbeads with microbead arraying, our microfluidic platform could offer a low-cost alternative to more complex flow cytometry-based methods, for applications including point-of-care (POC) diagnostics and on-site bio-chemical analysis [18, 19]. Furthermore, dynamic bead-based systems can be adapted for diverse chemical and bio-molecule detection assays (e.g., immunoassays [20]). To

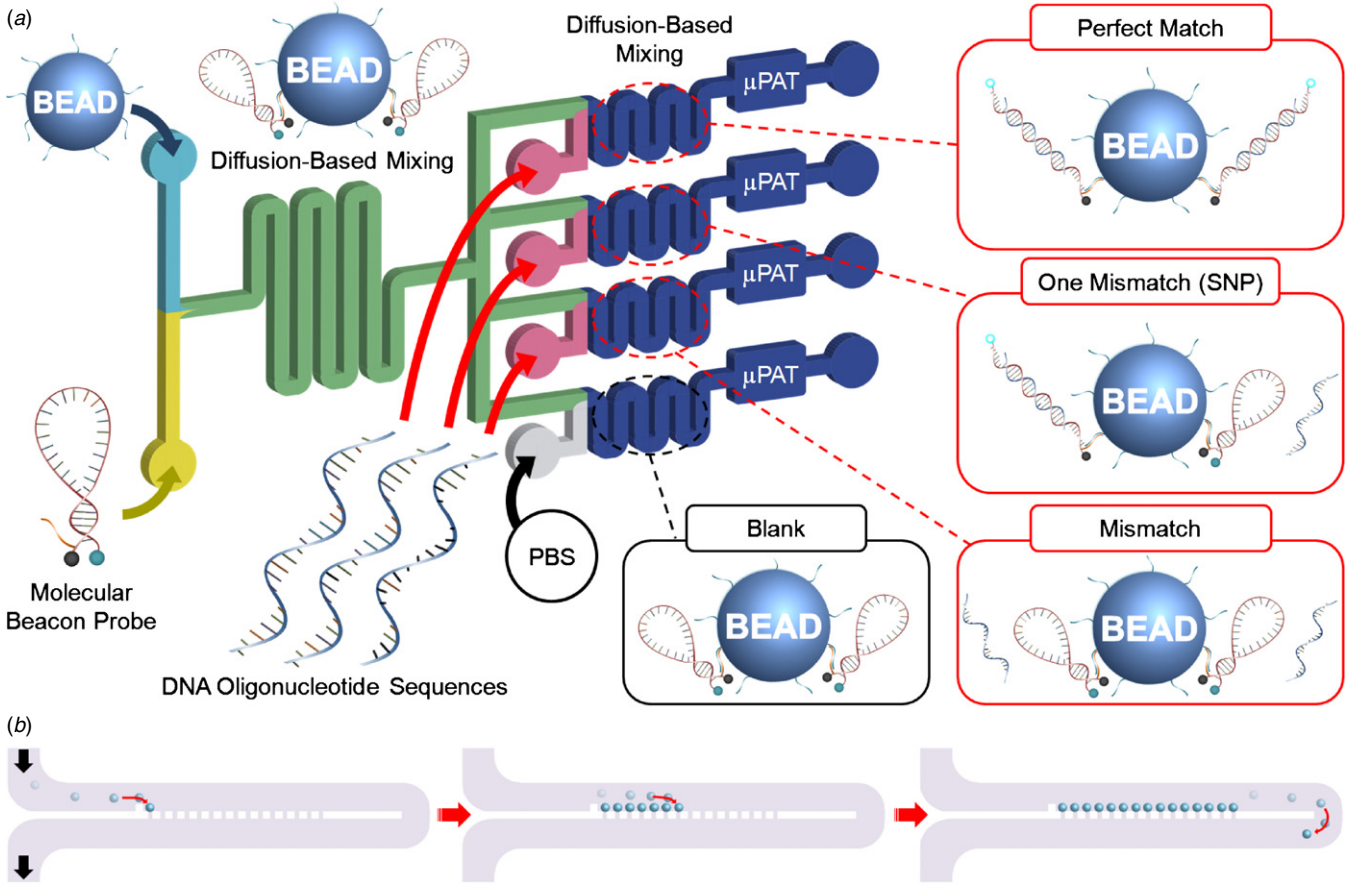

Figure 1. Conceptual illustrations of the dynamic bead-based microarray for parallel DNA detection. (*a*) Diffusion-based mixing in the microfluidic channel enables the immobilization of molecular beacon probes (MBs) on the microbead substrates. Three distinct DNA oligonucleotide sequences and PBS are inputted via separate inlets, each mixing independently with the MB-microbead solution. Hybridization occurs corresponding to the degree of matching between the MB and the DNA analytes, resulting in varying overall levels of fluorescence. After mixing, the microbeads are immobilized for fluorescence detection via micropost array trapping (μPAT). (*b*) Sequential illustrations of microbeads immobilizing in array positions via μPAT.

demonstrate our dynamic bead-based microarray platform, single nucleotide polymorphism (SNP) detection is achieved for single-stranded DNA (ssDNA) oligonucleotide sequences via molecular beacon probes (MBs) probes conjugated to polystyrene microbeads.

2. Design and working principle

2.1. Molecular beacon probes

Previously, MBs have been employed as a detection mechanism for target bio-molecules such as cytokines [21] and SNPs [22]. The MBs used for this study are ssDNA sequences containing a stem-and-loop structure, with a fluorophore and a quencher molecule on opposing ends. In the absence of a loop-complementary target DNA oligonucleotide sequence, the MBs maintain their stem-and-loop structure, which restricts fluorescence via a Förster Resonance Energy Transfer (FRET) interaction between the fluorophore and quencher molecules [23–26]. In the presence of a loop-complementary target sequence, the loop region of the MB hybridizes with the DNA oligonucleotide, which dissociates the stem structure. This conformational change positions the fluorophore and quencher molecules at a distance where FRET is no longer possible, enabling the fluorophore to fluoresce when excited [23–26]. The fluorescence response is reduced as the number of base-pair mismatches increases, thereby enabling the detection of SNPs for unlabeled DNA analytes [22].

2.2. Dynamic bead-based microarray for parallel DNA detection

Conceptual illustrations of the proposed dynamic microarray and reaction processes are shown in figure 1. MB-based genotyping is integrated with hydrodynamic microbead arraying to simultaneously detect multiple ssDNA oligonucleotide sequences in parallel. A suspension of polystyrene microbeads conjugated to an extended streptavidin-based linker and a solution of biotinylated MBs are loaded separately (figure 1(*a*)). Laminar diffusion-based mixing in the microfluidic channel enables MBs to bind to the surface of the microbead substrates and maintain a conformation with quenched fluorescence. Via separate inlets, four distinct homogeneous solutions are loaded: (i) *Perfect Match* (PM)—the target DNA oligonucleotide sequence, which is perfectly complementary

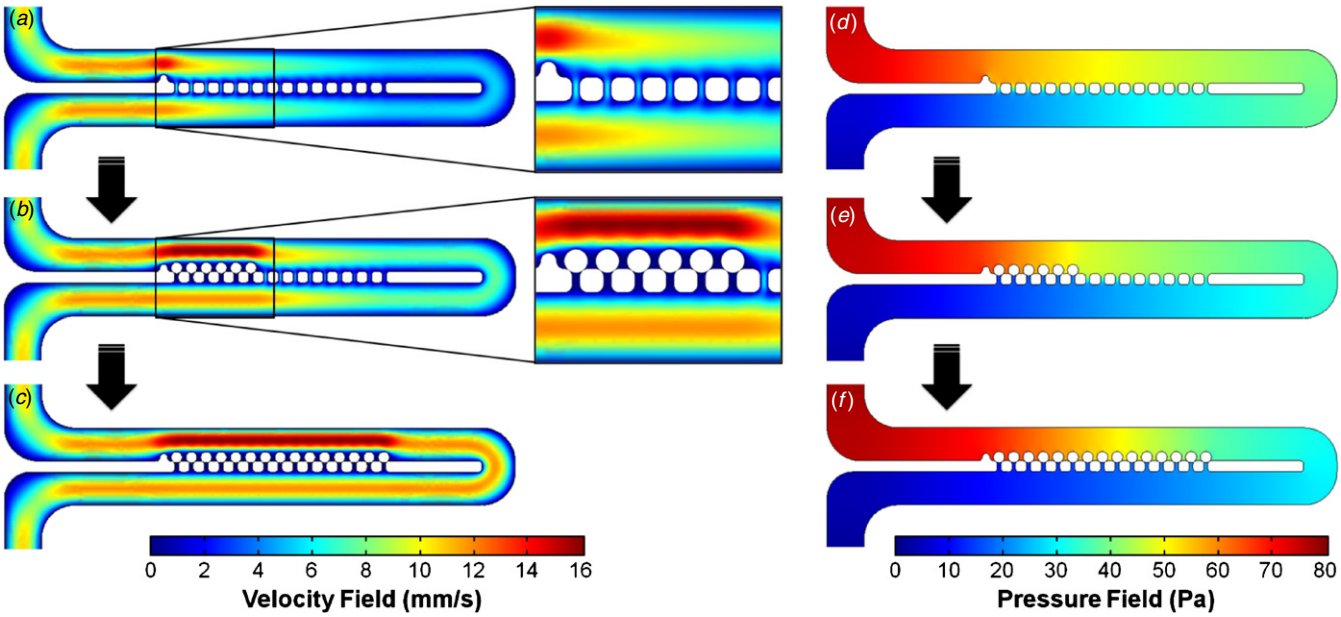

Figure 2. Sequential two-dimensional COMSOL fluid velocity field (*a*)–(*c*) and pressure field (*d*)–(*f*) simulations of microbeads arraying in the designated trapping sites between microposts via micropost array trapping (μPAT). (*a*)–(*c*) Fluid velocity field simulations of μPAT arrays (*a*) without any trapped microbeads, (*b*) with 6 trapped microbeads, and (*c*) with 15 trapped microbeads. (*d*)–(*f*) Pressure field simulations of μPAT arrays (*d*) without any trapped microbeads, (*e*) with 6 trapped microbeads, and (*f*) with 15 trapped microbeads.

Table 1. Names and sequences of the molecular beacon and DNA oligonucleotide sequences based on the hepatitis C viral (HCV) genome [27].

Name	Sequence
Molecular Beacon (MB)	5′-6-FAM-GCGAGC-CACCGGAATTGCCAGGACGACC-GCTCGC-BHQ-1–3′
Perfect Match (PM)	3′-GTGGCCTTAACGGTCCTGCTGG-5′
One Mismatch (SNP)	3′-GTGGCCTTAACGG**G**CCTGCTGG-5′
Mismatch (MM)	3′-GAGGGGCGGCGACTGGTGAG-5′

to the MB, (ii) *One Mismatch* (SNP)—a DNA oligonucleotide sequence with a single base-pair mismatch to the MB, (iii) *Mismatch* (MM)—a DNA oligonucleotide sequence with multiple base-pair mismatches, and (iv) *Blank*—a negative control solution of phosphate-buffered saline (PBS) (table 1) [7, 27]. The MB-microbead solution is distributed to four microchannels, each mixing independently with a singular DNA or PBS solution (figure 1(*a*)). When the MB-microbead solution is mixed with the PM solution, the complementary target DNA oligonucleotide sequences hybridize with the MBs, resulting in a detectable fluorescence on the surface of each microbead. After the MB-microbead solution is mixed with the SNP solution, the fluorescence response of the MBs is reduced due to the single base-pair mismatch. For the MM solution, the fluorescence response is further reduced due to the high number of base-pair mismatches between the analyte DNA and the MB. The blank solution provides a baseline reference value for the auto-fluorescence of the MBs on the microbead surface. To analyze the fluorescence response of the MBs corresponding to each solution, the microbeads are ultimately immobilized via a hydrodynamic arraying technique, termed micropost array trapping (μPAT).

2.3. Micropost array trapping

The development of dynamic bead-based microfluidic platforms for bio-molecule detection that preclude the need for flow cytometry equipment necessitates that microbeads be arrayed and immobilized for fluorescence visualization and signal detection [13, 28, 29]. Here, a μPAT technique is used to immobilize the microbeads after the reaction processes have come to completion (figure 1(*b*)). μPAT includes arrays of rectangular microposts in microfluidic channels that produce parallel flow paths for controlling microbead movement. Figures 2(*a*)–(*c*) show two-dimensional COMSOL fluid velocity field simulation results for μPAT systems with 0 (figure 2(*a*)), 6 (figure 2(*b*)) and 15 (figure 2(*c*)) immobilized microbeads. Initially, fluid flow through the gaps between microposts (i.e. trapping sites) is highest for the first vacant trap and decreases sequentially. The flow between microposts promotes the transport of motile microbeads to the designated trapping sites. When microbeads are immobilized at trapping locations, fluid flow through the occupied traps is obstructed, yielding increased flow rates to the remaining vacant sites. For example, figure 2(*a*) shows initial fluid velocities of 4.0 mm s^{-1} through the seventh trapping site; however, when microbeads immobilize in the first six trapping sites, the

fluid velocities through that same trapping site increase to 5.7 mm s^{-1} (figure 2(*b*)). This process continues until microbeads are immobilized at all of the trapping sites (figure 2(*c*)). As shown in the two-dimensional COMSOL pressure field simulations in figures 2(*d*)–(*f*), the pressure drop across the trapping sites enables microbeads to remain immobilized in the designated array positions after trapping. Additional microbeads that enter a μPAT system with fully trapped beads bypass the immobilized beads and are directed to subsequent μPAT arrays.

3. Materials and methods

3.1. Molecular beacon probe, DNA oligonucleotides and reagents

The biotinylated MBs were purchased from Biosearch Technologies, Inc. (Novato, CA). The MBs were terminally labeled with fluorescein (FAM) on the 5′ end of the probe, and a black hole quencher (BHQ-1) on the 3′ end (table 1). The PM, SNP and MM DNA oligonucleotide sequences were purchased from Invitrogen Corp. (Carlsbad, CA). All of the probes and DNA oligonucleotides were used without further purification or amplification. For the Blank solution, GIBCO™ Dulbecco's 1X PBS (#14287072; Invitrogen) was used.

3.2. Microbead functionalization

Streptavidin-coated 16 μm diameter polystyrene microbeads were purchased from Spherotech, Inc. (#SVP-150-4; Lake Forest, IL). An extended biological linker composed of biotinylated bovine serum albumin (BSA) and avidin, which were both purchased from Sigma-Aldrich Corp. (St. Louis, MO), was conjugated on the surface of the microbeads because the fluorescence response of bead-immobilized MBs is enhanced as the distance from the microbead surface is increased [7]. Laminar diffusion-based mixing facilitated the binding of biotinylated MBs to the microbead surface (i.e. microbead–streptavidin–biotinylated BSA–avidin–biotinylated MB).

3.3. Microdevice fabrication and design

The microfluidic device (2 cm × 3 cm) was fabricated via a standard soft lithography process. The negative photoresist, SU-8 2010 (MicroChem, Newton, MA), was spin-coated onto standard 4″ silicon wafers. Microfeatures were defined via contact photolithography (Hybralign, Series 400, Optical Associates, Milpitas, CA). Using the developed photoresist as a negative master, the device was micromolded with the silicone elastomer, poly(dimethylsiloxane) (PDMS), at a 10:1 ratio (Sylgard 184, Dow Corning, Corning, NY). After curing at 55 °C, the PDMS was removed and individual devices were cut from the PDMS. Ports for the catheter couplers (Instech Laboratories, Plymouth Meeting, PA) were punched at inlet and outlet locations. The PDMS devices were cleaned and covalently bonded to Fisherbrand glass microscope slides (Fisher Scientific, Pittsburgh, PA) via UV ozone treatment (UVO cleaner, model 42, Jetlight Company, Irvine, CA).

The microfluidic device was designed for 16 μm diameter microbeads. Due to the polydispersity of the microbeads, microchannel height and width were set at 18 and 50 μm, respectively. The MB-microbead mixing channel was 43 cm. Each of the MB-microbead-DNA/Blank mixing channels were 22 cm. For the μPAT arrays, the height of the systems remained 18 μm, the width of the channels were 45 μm, the microposts were 15 × 15 μm^2, and the gaps between microposts were 5 μm.

3.4. Fluid velocity field and pressure field simulations

Fluid velocity field and pressure field simulations were accomplished using the commercial finite element analysis software, COMSOL Multiphysics Version 3.5a. The 'Incompressible Navier–Stokes' application mode was used for both the two-dimensional and three-dimensional simulations. Based on the flow rate of fluid entering the μPAT arrays, the fluid velocity at the inlet was set at 7.8 mm s^{-1} for the velocity field simulations, and the pressure at the inlet was set at 80 Pa for the pressure field simulations. For all simulations, the pressure at the outlet was set at 0 Pa, while all other boundary conditions were set to have no-slip conditions. The mesh size was refined to ensure that the simulation results were independent of mesh size. The final mesh sizes ranged from 9871 to 10 138 elements for the two-dimensional simulations, and 17 797 to 21 251 elements for the three-dimensional simulations. Water was modeled in all of the fluidic simulations.

3.5. Experimental setup

All experiments were conducted under room temperature environment (20–25 °C) and without thermal cycling during device operation. To prevent the immobilization of microbeads at locations other than the designated trapping sites, the polysorbate surfactant, Tween 20 (20% in PBS, Fisher), was vacuum loaded into the device prior to operation. After a 15 min incubation period, four syringe pumps were used to load PBS into the device at a flow rate of 1 μL min^{-1} each via the PM, SNP, MM, and Blank inlets, until the Tween solution was removed from the device.

Six syringe pumps were used to independently control the input flow rates of each homogeneous solution or suspension (i.e. microbeads, MBs, PM, SNP, MM, and Blank). The flow rates for the microbead suspension (20 μL; 250 beads μL^{-1}) and the MB solution (20 μL; 10 μM) were each set at 0.60 μL min^{-1}, while the flow rates for the DNA oligonucleotide solutions (10 μL; 30 μM) and Blank solution (10 μL) were set at 0.17 μL min^{-1}. Laminar diffusion-based mixing of the MB-microbead solution and the MB-microbead-DNA/Blank solutions each occurred in separate serpentine microchannels. Once the μPAT arrays were filled with trapped microbeads, images were taken with a fluorescent inverted microscope (Motic AE31, Motic Instruments, Inc., Richmond, BC, Canada) connected to a Micropublisher 5.0 RTV charge-coupled device (CCD) camera (QImaging, Burnaby, BC,

Canada) and calibrated with QCapturePro (QImaging). All fluorescent images were captured at 100× magnification. The software, ImageJ (NIH, Bethesda, MD), was used to quantify the fluorescence response of each arrayed microbead (n = 624 microbeads from five distinct bead-based experiments) directly from the captured images. Since the contact between microbeads can distort the fluorescence response, data were excluded for microbeads that were in contact with other microbeads, or not immobilized in the designated trapping sites.

3.6. Relative fluorescent intensity quantification

Relative fluorescence intensities (RFIs) were quantified from fluorescent images of μPAT-immobilized 16 μm diameter microbeads. RFI values for individual microbeads were calculated as

$$\mathrm{RFI}_i = \frac{x_i - \overline{x}_{\mathrm{Blank}}}{\overline{x}_{\mathrm{PM}} - \overline{x}_{\mathrm{Blank}}}, \quad (1)$$

where x_i is the fluorescent intensity of a single microbead, $\overline{x}_{\mathrm{Blank}}$ is the mean fluorescent intensity of the microbeads that mixed with the Blank solution for the corresponding experiment, and $\overline{x}_{\mathrm{PM}}$ is the mean fluorescent intensity of microbeads that mixed with the PM solution for the corresponding experiment. The calculation of RFI values normalized the fluorescence results such that the mean RFI for the PM case was set at 1, while the mean RFI for the Blank case was set at 0.

3.7. Statistical analysis

Experimental results are presented as mean ± standard error of the mean (s.e.m.). The p values corresponding to differences in RFI between distinct DNA oligonucleotide sequences were calculated via one-way analysis of variance (ANOVA) and confirmed via unpaired Student's t tests. The p value corresponding to differences in RFI between the MM and Blank cases was calculated via unpaired Student's t tests because the mean RFIs for these cases were not assumed to be different. Differences with p values greater than or equal to 0.05 were not considered statistically significant.

4. Results and discussion

4.1. Parallel DNA detection via a dynamic bead-based microarray

The microfluidic bead-based platform was employed to: (i) immobilize solution-phase MBs onto the surfaces of microbeads and then (ii) mix the microbeads with four homogeneous solutions (i.e. PM, SNP, MM and Blank) in parallel to detect the flourescence response corresponding to each solution. Experimental results revealed that the microbeads with surface-immobilized MBs exhibited distinct and reproducible fluorescence intensities corresponding to each of the DNA oligonucleotide sequences (figures 3 and 4). Figure 3 shows fluorescence micrographs of μPAT-immobilized microbeads from a single experiment after

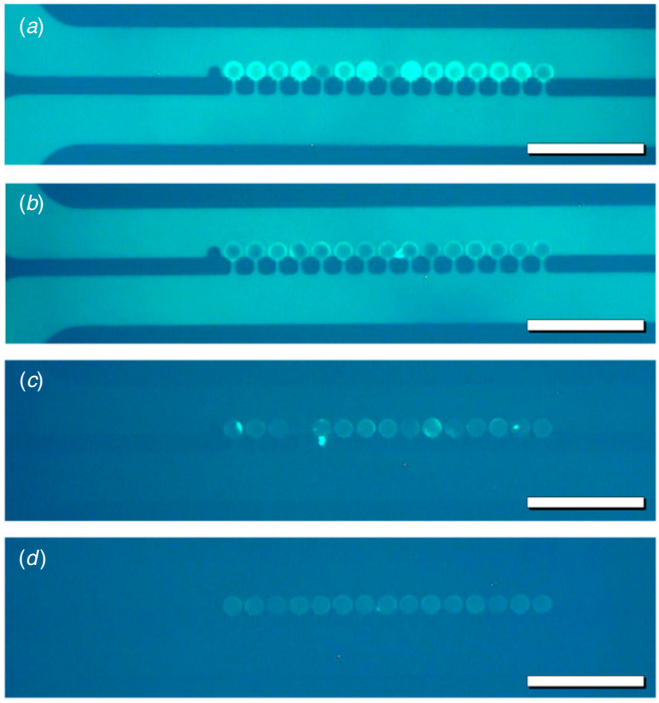

Figure 3. Fluorescence micrographs from a single experiment showing arrayed 16 μm diameter microbeads with surface-immobilized molecular beacon probes (MBs) after mixing with: (*a*) Perfect Match (PM), (*b*) One Mismatch (SNP), (*c*) Mismatch (MM) and (*d*) Blank (PBS) solutions. Scale bar = 100 μm.

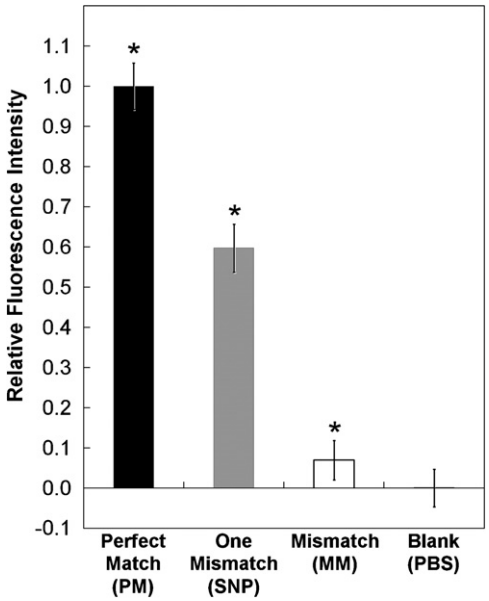

Figure 4. Relative fluorescence intensity (RFI) corresponding to Perfect Match (n = 148), One Mismatch (n = 194), Mismatch (n = 124), and Blank (n = 158) solutions. * denotes $p < 10^{-5}$ statistically significant differences. Error bars represent s.e.m.

mixing with the: (a) PM, (b) SNP, (c) MM and (d) Blank solutions in parallel. Prior to quantification, differences in fluorescence between the three DNA analytes can be observed visually. Solution phase MB–DNA hybridization occurred in the microchannels, which resulted in background fluorescence

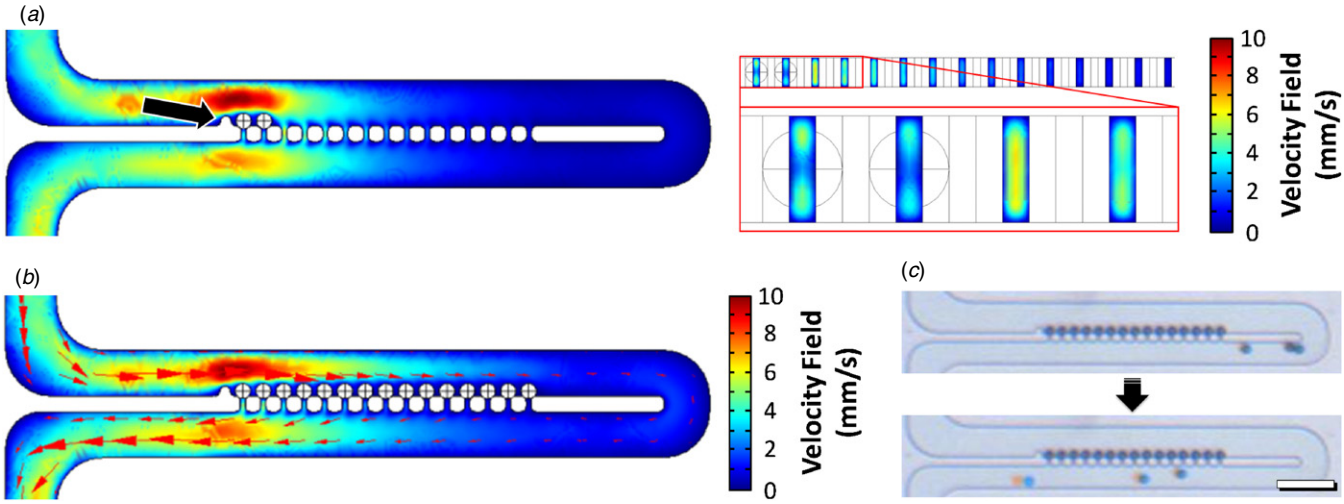

Figure 5. Effects of residual flow through occupied trapping sites on the micropost array trapping (μPAT) flow patterns. (*a*) Three-dimensional COMSOL fluid velocity field simulation with two arrayed microbeads. Cross-sectional view at half the height of a μPAT array (*left*), and cross-sectional view through the trapping sites, with an enlarged view of the first four traps (*right*). Black arrow marks the blocking protrusion. (*b*) Cross-sectional view at half the height of a μPAT array for a three-dimensional COMSOL fluid velocity field simulation with fully trapped microbeads. Red arrows mark the direction and magnitude of the fluid velocity field. (*c*) Sequential micrographs of three microbeads bypassing a μPAT array with fully trapped microbeads. Scale bar = 100 μm.

corresponding to the degree of matching between the MB and the DNA oligonucleotide sequences. However, because of the high fluorescence of the microbead-immobilized MBs, figure 4 shows that accurate and quantitative results were achieved without the need for additional time-consuming wash steps to eliminate the background noise.

The quantified fluorescence results are shown in figure 4. Each DNA oligonucleotide sequence was found to exhibit a statistically discernable RFI. Microbeads with surface-immobilized MBs that mixed with the PM solution produced the highest fluorescence response, with an average RFI of 1.00 ± 0.06. A single base-pair mismatch was found to significantly reduce the microbead fluorescence ($p < 10^{-5}$). The average RFI corresponding to the SNP solution was 0.60 ± 0.06. After mixing with the MM solution, microbeads exhibited an average RFI of 0.07 ± 0.05. The MM average RFI was distinguished from both the PM and SNP cases ($p < 10^{-5}$). In contrast, the MM average RFI was not discernable from the Blank case ($p = 0.31$), which demonstrates the specific binding of the MB. Microbeads that mixed with the PBS solution produced an average RFI of 0.00 ± 0.05. Thus, while the three DNA oligonucleotide sequences were observed to exhibit distinct fluorescence intensities, the fluorescence response corresponding to the MM and Blank solutions was not statistically distinguishable (figure 4).

4.2. *Micropost array trapping*

The μPAT technique was employed to achieve hydrodynamic immobilization of microbeads in array positions for fluorescence visualization and detection, thereby precluding the need for flow cytometry. After mixing with the four homogeneous solutions, 16 μm diameter microbeads were observed to array in the designated trapping sites between microposts. The number of microbeads (i.e. data points) immobilized via μPAT enabled oligonucleotide differentiation from single device runs. To increase the sample size for each experiment, several geometric considerations were found to enhance microbead arraying.

Ideally, the μPAT technique facilitates the transport of microbeads to vacant trapping sites, with the microbeads blocking all fluid flow through the occupied traps; however, when the spherical microbeads immobilize at the rectangular trapping locations, the flow through the traps is obstructed, but not blocked completely. For example, three-dimensional COMSOL fluid velocity field simulation results in figure 5(*a*) show fluid velocities up to 6 mm s^{-1} through the first occupied trap. Minimizing the microchannel height (i.e. with respect to the polydispersity of the microbead diameters) was found to limit the amount of residual flow through the occupied traps. One negative effect of the residual flow is that motile microbeads are directed to previously arrayed microbeads. When motile microbeads impact immobilized microbeads, chain reactions with additional microbead collisions can occur, releasing previously trapped microbeads. To prevent such collisions, a 10×10 μm^2 blocking protrusion (figure 5(*a*), *black arrow*) was included directly before the first trapping site of each μPAT array to divert subsequent microbeads away from previously arrayed microbeads, thereby limiting loss of data.

After microbeads immobilize in all of the trapping locations of a μPAT array, the residual flow through the occupied traps merges with the primary flow bypassing the trapping sites (figure 5(*b*)). As a result, fluid flow is redirected to the outer wall of the channel. Thus, when subsequent microbeads pass a μPAT array with fully trapped microbeads, they are transported to the outer wall (figure 5(*c*)). Due to this effect, for cases where the μPAT arrays were not alternated consecutively, microbead-immobilization in subsequent μPAT arrays was limited, as suggested by the flow streamlines in figure 6(*a*). In contrast, consecutively alternating the

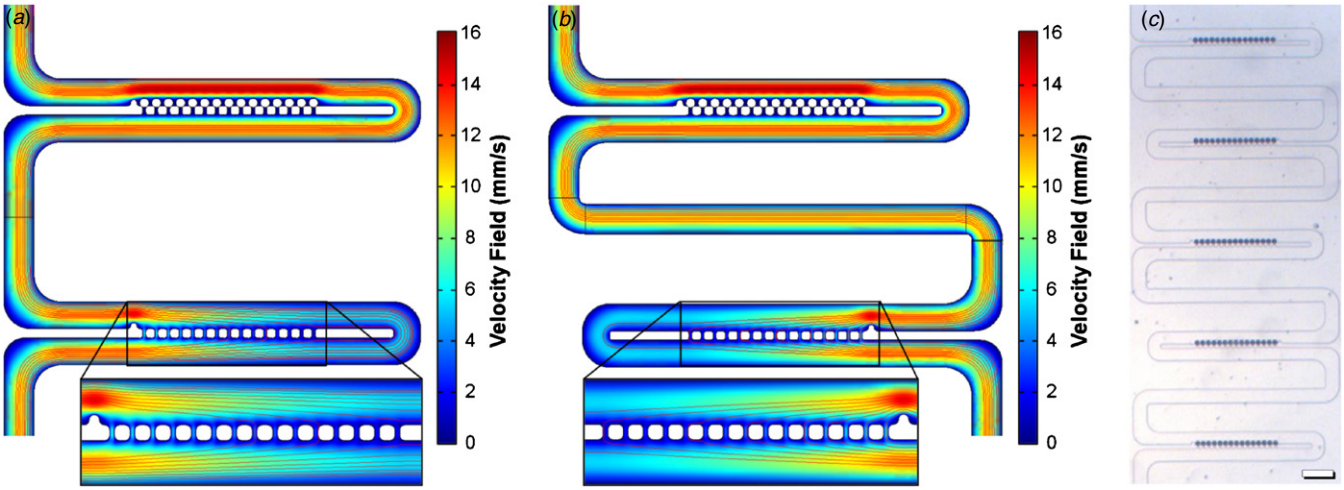

Figure 6. Non-alternating and alternating micropost array trapping (μPAT) configurations. (*a*) Two-dimensional COMSOL fluid velocity field simulation with overlaid fluid streamlines (*red lines*) for non-alternating μPAT arrays. The close-up view of the subsequent array shows two of eight fluid streamlines pass through the vacant trapping sites. (*b*) Two-dimensional COMSOL fluid velocity field simulation with overlaid fluid streamlines (*red lines*) for alternating μPAT arrays. The close-up view of the subsequent array shows seven of eight fluid streamlines pass through the vacant trapping sites. (*c*) Micrograph of 75 microbeads (16 μm in diameter) immobilized in alternating μPAT arrays. Scale bar = 100 μm.

μPAT arrays promoted microbead trapping in subsequent arrays, as suggested by the flow streamlines in figure 6(*b*). Experimentally, consecutively alternating the μPAT arrays was more effective for trapping microbeads in sequential μPAT arrays (figure 6(*c*)).

In this work, the fabricated system consisted of rectangular microchannels, which resulted in residual flow through trapping sites occupied by microbeads. Alternatively, the use of circular microchannels offers a potential means to resolve the issue of residual flow. However, by accomplishing microbead trapping without the need for circular channels, we were able to benefit from the advantages associated with one-mask soft-lithography processes, such as reduced costs, fabrication time and labor.

4.3. Microfluidic mixing

Laminar diffusion-based mixing occurred in the mixing channels for both the MB-microbead solution and the MB-microbead-DNA/Blank solutions. Based on syringe-pump controlled input flow rates of 0.60 μL min^{-1} for the MB and microbead solutions, and 0.17 μL min^{-1} for the DNA oligonucleotide and Blank solutions, the average fluidic velocity ($\overline{v}$) in each mixing channel was calculated as

$$\overline{v} = \frac{Q}{w \times h}, \tag{2}$$

where Q is the flow rate, w is the microchannel width and h is the microchannel height. The time required for full laminar diffusion (t_d) was calculated as

$$t_d = \frac{\left(\frac{w}{2}\right)^2}{2D}, \tag{3}$$

where D is the diffusion coefficient ($l_{\min} = \overline{v} \times t_d$, approximated as 60 μm^2 s^{-1} [30]). The minimum channel lengths ($l_{\min}$) required for complete laminar diffusion-based mixing were calculated for each of the mixing channels as

$$l_{\min} = \overline{v} \times t_d, \tag{4}$$

resulting in $l_{\min}$ values of 12 and 5 cm for the MB-microbead mixing channel and the MB-microbead-DNA/Blank mixing channels, respectively. As the lengths of the mixing channels in the fabricated device were 43 and 22 cm for the MB-microbead mixing channel and the MB-microbead-DNA/Blank mixing channels, respectively, complete laminar diffusion-based mixing was experimentally observed.

5. Conclusions

The integration of hydrodynamic microbead arraying techniques with dynamic microarrays offers a powerful and scalable technique for achieving low-cost detection of multiple bio-molecules in parallel. In this work, a microfluidic bead-based platform was employed to simultaneously detect multiple DNA oligonucleotide sequences via MBs conjugated to polystyrene microbead substrates. Label-free solutions of PM, SNP and MM DNA analytes were successfully differentiated in parallel with single base-pair mismatch specificity. Automated systems could be implemented to rapidly obtain fluorescence data from a single fluorescence image of μPAT-immobilized microbeads, serving as an effective alternative to more complex flow cytometry-based methods. While the current system was employed to detect four homogeneous solutions (PM, SNP, MM, and Blank), the present methodology can be modified to dramatically increase parallelization by distributing the microbeads to thousands of channels—each tailored for distinct reactions. The MB used in this study was designed to detect single nucleotide differences in ssDNA oligonucleotide sequences; however, prior works have demonstrated that MBs can be used as a detection

mechanism for diverse chemicals and bio-molecules. Thus, the dynamic bead-based microarray presented in this work could be adapted to achieve multiplexed detection for a wide range of biological applications, such as POC diagnostics, drug screening and pathogen detection.

Acknowledgments

The authors would like to acknowledge Armon Mahajerin, Barthélémy Lüthi, Kosuke Iwai, David De Renzy, Parminder Singh, Paul Lum, Joanne C Lo, Adrienne T Higa, Brian D Sosnowchik, Hansang Cho, and John Waldeisen for their contributions. This project is partially supported by the DARPA N/MEMS Fundamental program.

References

[1] Syvanen A C 2001 Accessing genetic variation: genotyping single nucleotide polymorphisms *Nature Rev. Genet.* **2** 930–42
[2] Verpoorte E 2003 Beads and chips: new recipes for analysis *Lab Chip* **3** 60N–68N
[3] Dittrich P S and Manz A 2006 Lab-on-a-chip: microfluidics in drug discovery *Nature Rev. Drug Discovery* **5** 210–8
[4] Tan W H and Takeuchi S 2007 A trap-and-release integrated microfluidic system for dynamic microarray applications *Proc. Natl Acad. Sci. USA* **104** 1146–51
[5] Lim C T and Zhang Y 2007 Bead-based microfluidic immunoassays: the next generation *Biosens. Bioelectron.* **22** 1197–204
[6] Nilsson J, Evander M, Hammarstrom B and Laurell T 2009 Review of cell and particle trapping in microfluidic systems *Anal. Chim. Acta* **649** 141–57
[7] Horejsh D, Martini F, Poccia F, Ippolito G, Di Caro A and Capobianchi M R 2005 A molecular beacon, bead-based assay for the detection of nucleic acids by flow cytometry *Nucleic Acids Res.* **33** e13
[8] Ng J K K and Liu W T 2006 Miniaturized platforms for the detection of single-nucleotide polymorphisms *Anal. Bioanal. Chem.* **386** 427–34
[9] Du J Y *et al* 2009 Bead-based profiling of tyrosine kinase phosphorylation identifies src as a potential target for glioblastoma therapy *Nature Biotechnol.* **27** 77–83
[10] Dunbar S A 2006 Applications of luminex (r) xmap (tm) technology for rapid, high-throughput multiplexed nucleic acid detection *Clin. Chim. Acta* **363** 71–82
[11] Ali M F *et al* 2003 DNA hybridization and discrimination of single-nucleotide mismatches using chip-based microbead arrays *Anal. Chem.* **75** 4732–9
[12] Hashmi G *et al* 2005 A flexible array format for large-scale, rapid blood group DNA typing *Transfusion* **45** 680–8
[13] Ng J K, Feng H H and Liu W T 2007 Rapid discrimination of single-nucleotide mismatches using a microfluidic device with monolayered beads *Anal. Chim. Acta* **582** 295–303
[14] Qiu X B *et al* 2009 Finger-actuated, self-contained immunoassay cassettes *Biomed. Microdevices* **11** 1175–86
[15] Steemers F J and Gunderson K L 2007 Whole genome genotyping technologies on the BeadArray (TM) platform *Biotechnol. J.* **2** 41–9
[16] Thompson J A and Bau H H 2010 Microfluidic, bead-based assay: theory and experiments *J. Chromatogr. B-Anal. Technol. Biomed. Life Sci.* **878** 228–36
[17] Thompson J A, Du X G, Grogan J M, Schrlau M G and Bau H H 2010 Polymeric microbead arrays for microfluidic applications *J. Micromech. Microeng.* **20** 115017
[18] Hur S C, Tse H T K and Di Carlo D 2010 Sheathless inertial cell ordering for extreme throughput flow cytometry *Lab Chip* **10** 274–80
[19] Kim D N, Lee Y and Koh W G 2009 Fabrication of microfluidic devices incorporating bead-based reaction and microarray-based detection system for enzymatic assay *Sensors Actuators* B **137** 305–12
[20] Nagai H, Narita Y, Ohtaki M, Saito K and Wakida S I 2007 Single-bead analysis on a disk-shaped microfluidic device using an antigen-immobilized bead *Anal. Sci.* **23** 975–9
[21] Tuleuova N, Jones C N, Yan J, Ramanculov E, Yokobayashi Y and Revzin A 2010 Development of an aptamer beacon for detection of interferon-gamma *Anal. Chem.* **82** 1851–7
[22] Hsieh A T H, Pan P J H and Lee A P 2009 Rapid label-free DNA analysis in picoliter microfluidic droplets using fret probes *Microfluid. Nanofluid.* **6** 391–401
[23] Strohsahl C M, Miller B L and Krauss T D 2007 Preparation and use of metal surface-immobilized DNA hairpins for the detection of oligonucleotides *Nat. Protoc.* **2** 2105–10
[24] Kim S *et al* 2007 Rapid DNA hybridization analysis using a PDMS microfluidic sensor and a molecular beacon *Anal. Sci.* **23** 401–5
[25] Jung J *et al* 2007 Fast and sensitive DNA analysis using changes in the FRET signals of molecular beacons in a PDMS microfluidic channel *Anal. Bioanal. Chem.* **387** 2609–15
[26] Tan L *et al* 2005 Molecular beacons for bioanalytical applications *Analyst* **130** 1002–5
[27] Yang J H, Lai J P, Douglas S D, Metzger D, Zhu X H and Ho W Z 2002 Real-time RT-PCR for quantitation of hepatitis C virus RNA *J. Virol. Methods* **102** 119–28
[28] Zuo X B, Yang X H, Wang K M, Tan W H and Wen J H 2007 A novel sandwich assay with molecular beacon as report probe for nucleic acids detection on one-dimensional microfluidic beads array *Anal. Chim. Acta* **587** 9–13
[29] Ng J K, Selamat E S and Liu W T 2008 A spatially addressable bead-based biosensor for simple and rapid DNA detection *Biosens. Bioelectron.* **23** 803–10
[30] Nkodo A E *et al* 2001 Diffusion coefficient of DNA molecules during free solution electrophoresis *Electrophoresis* **22** 2424–32